Biophysical Journal
Biophysical Perspective

Biophysical Society

On the Quantification of Cellular Velocity Fields

Dhruv K. Vig,[1] Alex E. Hamby,[1] and Charles W. Wolgemuth[1,*]
[1]Departments of Physics and Molecular and Cellular Biology, University of Arizona, Tucson, Arizona

ABSTRACT The application of flow visualization in biological systems is becoming increasingly common in studies ranging from intracellular transport to the movements of whole organisms. In cell biology, the standard method for measuring cell-scale flows and/or displacements has been particle image velocimetry (PIV); however, alternative methods exist, such as optical flow constraint. Here we review PIV and optical flow, focusing on the accuracy and efficiency of these methods in the context of cellular biophysics. Although optical flow is not as common, a relatively simple implementation of this method can outperform PIV and is easily augmented to extract additional biophysical/chemical information such as local vorticity or net polymerization rates from speckle microscopy.

Large-scale coordinated motion is ubiquitous in cell biology. Indeed, cytoskeletal flow within a single cell is due to the movement of molecules, and, similarly, individual cells can adhere to one another and form multicellular conglomerates that exhibit fluid-like motion (1). Time-lapse images at either of these cellular length scales show persistent features that move with the intramaterial flow. For example, in speckle microscopy, the locations of bright spots in an image correspond to the positions of single or multiple fluorescently labeled F-actin molecules (2). Previous studies have utilized single-particle tracking (SPT) methods to follow the movement of each speckle, thereby extracting the F-actin flow (3). SPT has also been used to track individual cells during wound-healing assays (4,5), producing cell trajectories that follow the bioflow. However, when the displacement of a particle exceeds the average interparticle spacing, the use of SPT to properly identify individual particles from frame to frame becomes computationally difficult or even impossible (2).

An alternative is to use flow visualization methods that determine the "best guess" for the displacements of subregions within the image between subsequent frames (6). That is, rather than identifying and tracking individual features in time-lapse images, flow visualization techniques effectively compute the average motion over a few too many features. In cell biology and biophysics, the most common of these techniques is particle image velocimetry (PIV) (7), which has been used to quantify the internal cytoskeletal movements that drive cell migration and mitosis (8,9); the collective migration of mammalian cells during development, tissue remodeling, wound healing, and cancer (1,10–12); and the fluid-like behavior of dense suspensions of bacteria (13,14). PIV has also been employed to map cytoplasmic flow in embryos (15) and used in conjunction with SPT methods to track bead displacements in traction force microscopy (16).

The extensive usage of PIV in cellular biology has suppressed other methodologies for flow extraction, and many researchers may not be aware that other modalities are available. One such alternative is optical flow constraint (17). Here, we review and benchmark PIV and optical flow constraint within the context of modern cell biology and biophysics research. We find that optical flow is more accurate and efficient than PIV. This methodology, then, needs more exposure within the biophysics community, as flow field reconstruction is crucial for defining how force and movement are connected in extended biological systems, and is also necessary for quantitatively validating mathematical models and testing their predictions.

A brief introduction to SPT, PIV, and optical flow

At a basic level, SPT is the most conceptually simple methodology for tracking motion in a sequence of images. Individual features in a frame (e.g., the signals from fluorescently labeled proteins) are identified and labeled. In each subsequent frame, the location of those features is notated and the distance that each particle has moved is then easily quantified. Because individual motions of particles are being tracked, this method can handle movements that vary over short spatial distances, such as random or chaotic motion. However, because the features that are being tracked

Submitted July 21, 2015, and accepted for publication February 15, 2016.
*Correspondence: wolg@email.arizona.edu
Editor: Brian Salzberg.
http://dx.doi.org/10.1016/j.bpj.2016.02.032

are often similar in appearance, as the number of particles or features increases, it becomes increasingly difficult to accurately determine which feature at one time corresponds to the same feature at a later time. This problem can be confounded due to particle disappearance or particle merging or splitting (18). Although many of these problems can be overcome for moderate object densities, the computational time required to accurately track the particles is limiting and the method still can break down at high densities (18). In addition, when the features are not point-like (e.g., when tracking movement in a confluent layer of cells), it may not be possible to consistently identify specific persistent features.

Instead of tracking individual features, PIV and optical flow seek to identify the average movements of subregions in the image. Therefore, these methods are more robust to noise in the images, but are not able to capture high-frequency movements that occur over small spatial distances. Both of these methods compare the intensity distribution in a subregion of the image with the intensity profiles obtained at later time points to minimize (or maximize) a specified quantity (which can be considered to be a cost function).

PIV assumes that if the flows are smooth enough, nearby features in the image will stay in a relatively similar orientation with respect to each other from one frame to the next. Therefore, we want to find the subregion in a subsequent image where the particle orientations match best with the subregion at the current time. PIV uses correlation functions to determine this best guess for the displacements of subregions between two subsequent images (Fig. 1, *A* and *B*) (a fairly extensive description of PIV and its applications is given in (7)). In this method, the user defines an interrogation window, which typically is a square domain of size $N \times N$ pixels. Subregions the size of the interrogation window are excised from one image and then rastered over a subsequent image. At each position of the raster, the correlation between the excised subregion (region 1) and the overlapped region (region 2) is computed as

$$C(i,j) = \frac{\sum_{\text{region 1}} \sum_{\text{region 2}} \left(I_1(k,l) - \bar{I}_1\right)\left(I_2(k+i,l+j) - \bar{I}_2\right)}{\sqrt{\sum_{\text{region 1}} \left(I_1(k,l) - \bar{I}_1\right)^2 \sum_{\text{region 2}} \left(I_2(k+i,l+j) - \bar{I}_2\right)^2}}, \tag{1}$$

where $I_{1,2}$ is the intensity in region 1 or 2, respectively, and $\bar{I}$ denotes the average intensity in the subregion. The displacement of the subregion from its original location is (i,j). Because the correlation function compares the intensity difference from the average intensity, when two bright regions or two dark regions overlap, there is a positive contribution to the correlation function. However, when a light region overlaps with a dark region, there is a negative contribution to the correlation. Consequently, the correlation is maximized when there is the most overlap between the two regions. The location of this peak in the correlation then defines how far the subregion has moved between the two images (i.e., the displacement vector) (Fig. 1 *B*). Typically, the peak is fitted to either a quadratic or Gaussian function to obtain subpixel resolution of the peak location (7). Because PIV makes a statistical comparison between the two images, it relies on having sufficient information within each subregion to accurately determine the displacement. Therefore, the size of the interrogation window needs to be chosen so that each subregion contains multiple particles. One drawback to PIV is that detection of the cross-correlation peak is susceptible to errors, especially when the signal/noise ratio is low (19). Therefore, it is necessary to identify and remove erroneous vectors (19). A method for reducing errors is multipass PIV, in which a large box size is used to coarsely determine the displacements. One can then refine the displacement field by subsequently iterating with decreasing box sizes (7), thus improving the accuracy but also increasing the computation time (Fig. 1 *A*). If the velocity field is assumed to be quasi-stationary (i.e., it does not vary much over a few frames), multiple frames can be used to define the correlation function, which can greatly enhance the accuracy and spatial resolution of PIV (20).

Optical flow constraint, developed by Lucas and Kanade (17), is based on the physical/mathematical description for flow-driven transport, the advection equation (Fig. 1 *B*). In microscope images, information about the locations of objects is encoded in the intensity in the image, regardless of the imaging modality. Movement of the objects with local velocity v transports the image intensity profile I. Therefore, over small but finite time differences Δt, the change in the intensity is described by

$$\frac{\Delta I}{\Delta t} = \frac{I(t+\Delta t) - I(t)}{\Delta t} = -\mathbf{v} \cdot \nabla I. \tag{2}$$

This equation assumes that the objects do not move by substantial distances between images. To allow the methodology to work for larger displacements, the images can be blurred using a Gaussian function with a standard deviation that we denote as *BlurSTD* (Fig. 1 *C*). In the advection equation, information about the velocity is effectively transmitted to subsequent times by the gradient in the image. Blurring the images acts to spread this information out over larger distances. Blurring can also be considered as a form of subsampling the images, which is known to improve the optical flow method (21,22). Based on these arguments, the *BlurSTD* should be comparable to the characteristic velocity multiplied by the time between images (Fig. 1 *C*). Using the blurred images, the image at one time is then subtracted from an image at a later time and the gradient is calculated using the average intensity at both time points. Finally, the velocities in subregions of the image are determined by minimizing the squared residuals of Eq. 2 in the subregion using a least-squares method (LSM) (17).

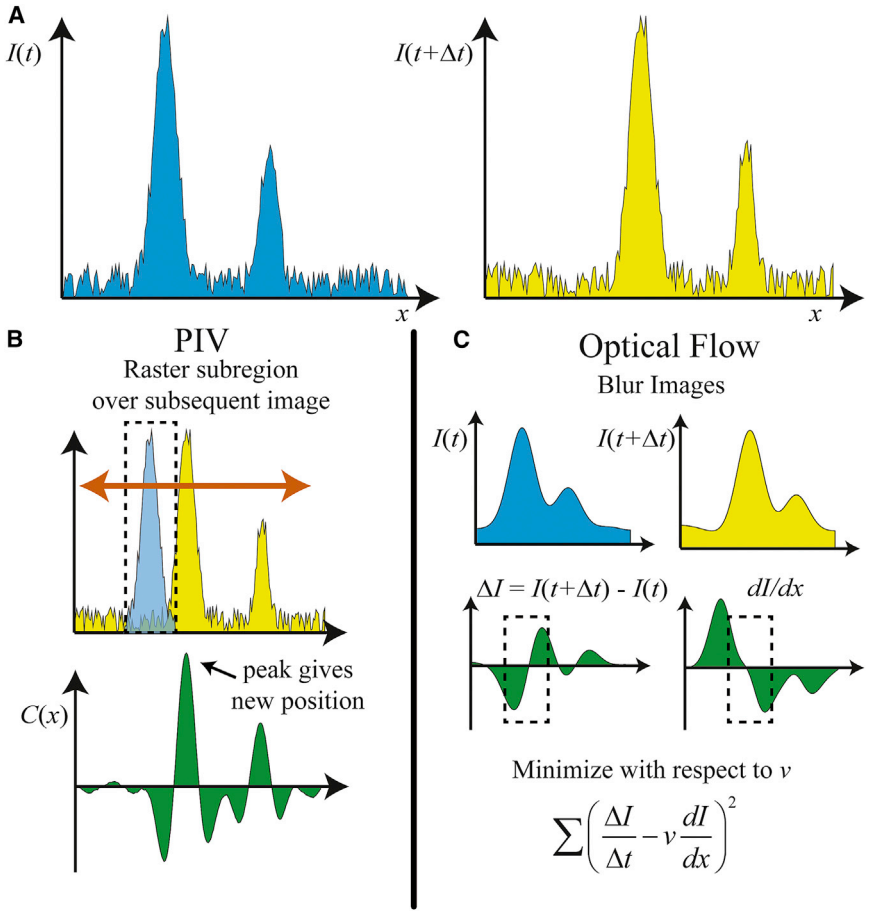

FIGURE 1 Techniques for flow extraction. (*A*) One-dimensional illustration of the intensity in an image at time t (*blue*) and $t + \Delta t$ (*yellow*), corresponding to the net rightward motion of two bright features. (*B*) In PIV the user defines an interrogation area that encompasses identifiable features within the image. This region (*dashed line*) at time t is then rastered over the image at $t + \Delta t$ and the cross-correlation function is used to determine the best match for the new location of that feature. (*C*) Optical flow constraint uses the change in intensity between two images along with the intensity gradient to determine the velocity. The image intensity is first blurred to spread out information in the image over a larger region (i.e., to produce greater overlap between the image features at t and $t + \Delta t$). The change in intensity is then described by Eq. 1, and one uses an LSM to determine the velocities within subregions of the image by computing the change in intensity and intensity gradients from processed image pairs. To see this figure in color, go online.

Blurring in this method is a means of regularizing the estimated velocity field. An alternative or additional method for regularization in the context of optical flow involves adding an additional cost function that minimizes the gradient in the velocity field (23). It is also possible to use a recursive or hierarchical analysis, sometimes known as a pyramid method, that coarsely determines the velocity field using a highly blurred or subsampled image, and then gradually refines the velocity measurements by shifting subregions in the image using the coarse velocity field and then using a less blurred image to more accurately capture the small-scale flows (21,22). This recursive method is analogous to multipass methods for PIV.

Accuracy and efficiency of velocity field measurements

There have been a few head-to-head comparisons between PIV and optical flow constraint (22,24). Since the use of PIV is widespread within the biophysics and cell biology communities, we were surprised to find that these comparisons typically show that optical flow constraint outperforms PIV in both accuracy and efficiency. However, these comparisons were not made within the context of images typically obtained in cell biology research, so we chose to benchmark the methods with multiple synthetic movies that we created to represent the motion of ellipsoidal particles at a range of densities within different flow fields acquired by either epifluorescence or differential interference contrast (DIC) microscopy. Here we describe the results from three of these synthetic movies (Fig. 2, *a–c*; Movies S1, S2, and S3 in the Supporting Material). We observed the same trends in all of our other test cases as well. The flow fields in each movie were determined using optical flow and PIV (25) with single-pass and four-pass fast Fourier transform window deformation. We computed the accuracy of the three methods using the L^2-norm (Fig. 2 *c*). In all cases, optical flow and four-pass PIV had substantially better accuracy than single-pass PIV. Optical flow was also significantly more accurate than four-pass PIV in all cases except for spatially uniform motion (i.e., pure translation). In addition, single-pass and four-pass PIV exhibited more variation between frames than optical flow, suggesting that PIV is prone to more errors than optical flow (Fig. 2 *d*). Finally, we tested the efficiency of optical flow and single- and four-pass PIV by measuring each method's computation time for various image sizes. We found that on average, optical flow was ~2–3 times faster

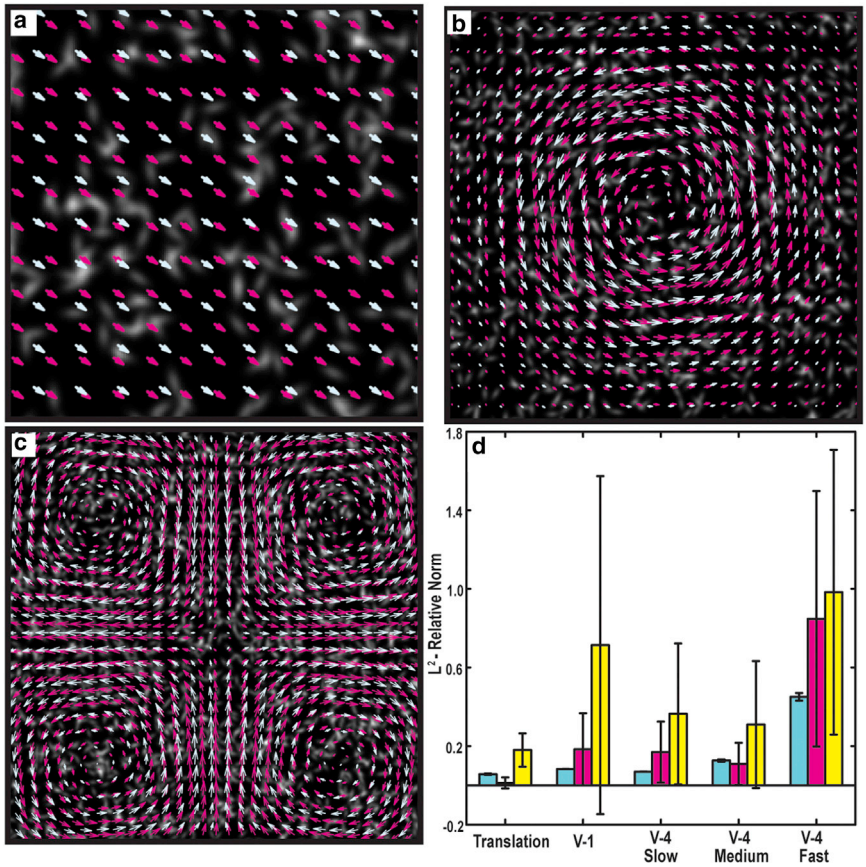

FIGURE 2 Validation of optical flow (*cyan*) and single-pass (*yellow*) and four-pass (*magenta*) PIV. (*a–c*) The accuracy of each methodology was determined by computing flow fluids from synthetic movies exhibiting (*a*) spatially uniform motion, (*b*) a dilute density of particles rotating in a single vortex, and (*c*) a dense population of particles rotating in multiple vortices. The overlays show discrepancies between optical flow and four-pass PIV. (*d*) L^2-relative norm errors for all test cases. To see this figure in color, go online.

than single-pass PIV and 29 times faster than four-pass PIV (Table 1).

Biological applications and extensions

Our results from analyzing the synthetic movies suggest that optical flow constraint outperforms PIV, which is consistent with previous findings (22,24), but how well do each of these methodologies handle real biological data? The difficulty with this question is that in most scenarios the ground truth of the flow is not known. By eye, we can often pick out the direction of flow on a coarse scale, which can be used to qualitatively evaluate the computed velocity field. However, this does not provide a good means for evaluating the finer structure of the velocity field, nor does it allow one to judge whether the magnitudes of the computed velocities are correct. In our own work, we have found that although we can sometimes get reasonable-looking velocity fields, the magnitudes of the velocity are off substantially.

TABLE 1 Efficiency of Optical Flow Compared with PIV

Image Size (Height × Width)	Computation Time Cost (in Seconds)		
	Optical Flow	One-Pass PIV	Four-Pass PIV
128 × 128	0.387	2.393	N.A.
256 × 256	0.746	2.617	19.678
512 × 512	2.879	6.026	81.424
1024 × 1024	11.806	20.574	385.713
2000 × 2000	46.473	73.812	1341.235

If we are going to use extracted velocity fields to quantify the dynamics of biological systems and/or to test predictions from mathematical models of cellular mechanisms, we must have a way to validate the outputs of these algorithms when the real flow field is not known. Here, we suggest a method to address this issue: simulating synthetic tracer particles in the computed velocity field and overlaying the position of the particles onto the original time-lapse images. If the locations of the particles follow the motion of nearby identifiable features in the images, one can be fairly confident that the extracted velocity fields are reasonably accurate. We implement this method by randomly seeding 100 tracer particles into the first frame of a movie. The corresponding velocity field for the first image is then interpolated onto the particle positions and the position of the particle is updated using a forward Euler time-stepping routine. This process is repeated for all frames of the movie and any particles that flow out of the image domain are excluded. This approach is especially useful for images acquired by DIC microscopy, where tracking individual cell trajectories is notoriously difficult (10).

We used this methodology to examine how well optical flow constraint and PIV performed in quantifying bioflows

in two common biological scenarios: confluent epithelial layers (Fig. 3 *a*), and dense suspensions of *Escherichia coli* (Fig. 3 *b*). For confluent epithelial layers, this analysis revealed that although both the single-pass and four-pass PIV methods were able to generate reasonable-looking flow fields, they were unable to continuously follow the motion of the cells (Fig. 3 *a*). In contrast, using velocity fields that were computed by optical flow with image blurring produced particle trajectories that accurately followed features in the images; however, if the image was not preblurred, optical flow broke down, producing velocity fields that were near zero (Fig. 3 *a*). For dense suspensions of *E. coli*, we found that preblurring did not degrade the velocity as significantly as it did for the confluent epithelial cells. This is because these images were captured at 32 fps and the bacteria moved at ~30 μm/s. Therefore, the average displacement of a bacterium between frames was smaller than the size of the bacterium. An interesting feature of the tracer particle dynamics in these movies is that although single-pass PIV, four-pass PIV, and image-blurred optical flow all produced approximately similar velocity fields, tracer particles that were simulated using one of the flow fields could end up far from a tracer particle that was started in the same position but updated using a velocity field that was extracted by a different method. Careful inspection of the movies suggests that all of these methods computed the velocities reasonably well, but the chaotic nature of the flows in these dense bacterial suspensions led to large discrepancies in the tracer particle trajectories (Fig. 3 *b*; Movie S5).

These results suggest that although PIV can be accurate in some instances, optical flow provides a more robust method for tracking bioflows. An added benefit of optical flow is that it is straightforward to augment Eq. 2 to extract additional information. For example, local vorticity or shearing flows can be determined by adding spatial dependence to the velocity field (17), or a reaction term can be added to determine local density changes (3,26). The latter extension may be relevant for speckle microscopy, where polymerization or depolymerization of actin locally adds or removes particles (9). In regard to the advection equation (Eq. 2), the creation or destruction of particles is mathematically represented by an additional source term. If we treat this source term as a scalar quantity that is positive (negative) when polymerization (depolymerization) exceeds depolymerization (polymerization), then adding a source term γ to Eq. 2 should allow the optical flow method to simultaneously determine the velocity field and the local assembly rate, as has been done in the context of actin dynamics (3,26):

$$\frac{\Delta I}{\Delta t} = -\mathbf{v} \cdot \nabla I + \gamma. \tag{3}$$

The residuals of this equation are then minimized with respect to the two components of the velocity and the source term using an LSM. We tested the accuracy of this method

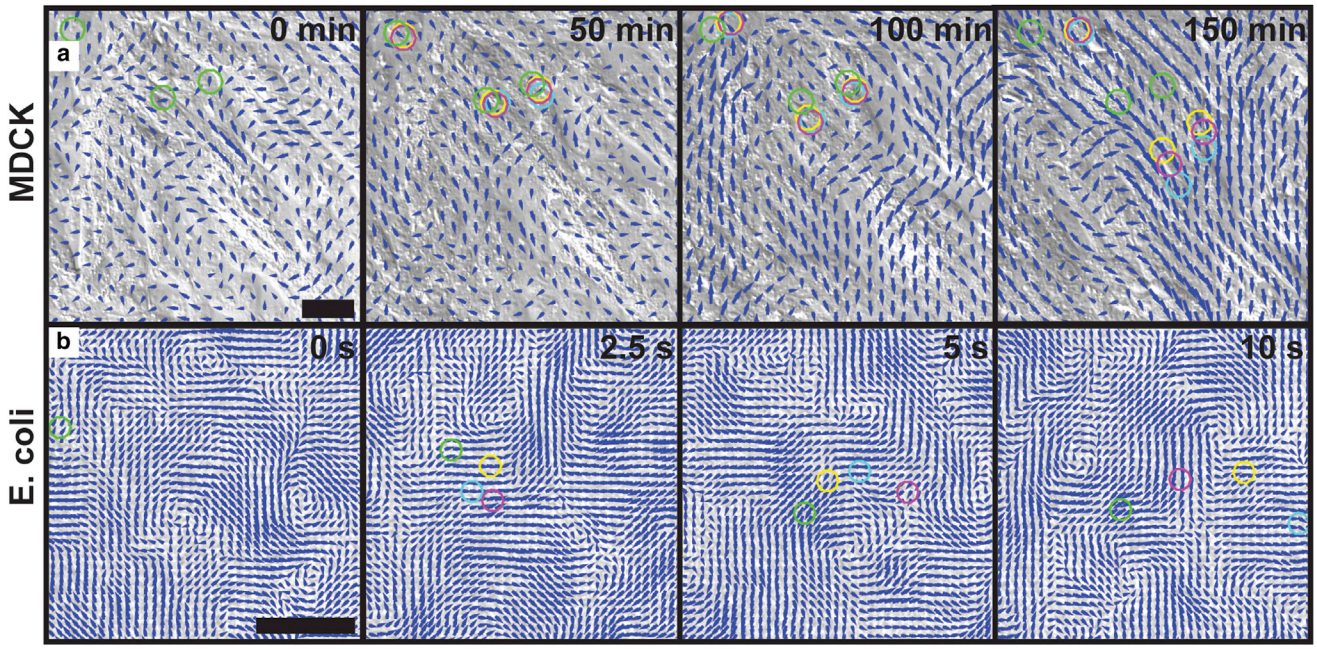

FIGURE 3 Recreating flows in collective cell migration using tracer particles. (*a* and *b*) The trajectories of simulated tracer particles, calculated from velocity fields extracted by optical flow using blurred (*cyan*) or unblurred (*green*) images, or extracted using single-pass (*yellow*) or four-pass (*magenta*) PIV, were used to determine the accuracy of the measured flow displacements in (*a*) confluent MDCK type I monolayers (scale bar, 50 μm) and (*b*) dense suspensions of *E. coli* (scale bar, 50 μm). These tracer particles are overlaid on the velocity field (*blue*) that was extracted using optical flow with blurring. To see this figure in color, go online.

by creating a synthetic movie in which fluorescent ellipsoid-shaped particles were transported by a set velocity field and stochastically added or removed using prescribed polymerization and depolymerization rates (Fig. 4 *a*). We found that optical flow with the added reaction term was able to sufficiently capture the local net polymerization rates of the particles. We also tested this version of optical flow against previously measured net assembly rates of F-actin in fluorescent speckle microscopy movies (9). Indeed, optical flow with a reaction term was able to qualitatively reproduce the previously measured net assembly rates of F-actin (Fig. 4, *b* and *c*). These results are in agreement with previous studies in which optical flow was applied with a source/sink term to extract speckle flow fields (3,26).

CONCLUSIONS

Accurate measurements of large-scale flows within cells and cell collectives provide key information that allows one to determine the biophysics of cellular transport and motility. In addition, these data can be integrated with biochemical perturbations or biosensors to help reveal mechanochemical mechanisms in cell biology (4,27,28). SPT techniques and PIV have been the principal means for analyzing bioflows in the cellular biophysics and cell biology communities. The computer vision community, though, has developed other alternatives that have not received the same notice or usage. Here we focused on optical flow constraint, a method developed by Lucas and Kanade (17) in 1981. In our own research, we found that this algorithm was easy to implement, took less time to run, and provided velocity fields that were roughly comparable to the output from PIV (25). Therefore, we sought to determine which of these methods is more accurate. Despite the broad use of PIV in cell biology, we found that optical flow is more accurate and can be substantially more efficient than PIV. It is not surprising, then, that optical flow is already being extensively applied in traditional hydrodynamic studies (29,30) outside of biology.

An aspect of optical flow constraint that greatly appeals to us is the fact that it is based on the physics of transport. Because of this, if other physical processes are also known to be at play in a system, it is straightforward to augment the transport equation to include these additional processes, as we showed using a source term to extract net polymerization rates from speckle images. However, whatever method is used, we feel it is important for researchers to test how well that method recreates the flow. One method, proposed here, is to use simulated tracer particles to determine whether the flow fields correspond to identifiable features in the images.

From our perspective, the biophysics and cell biology communities should not be so reliant on PIV and should be aware of other methods such as optical flow constraint.

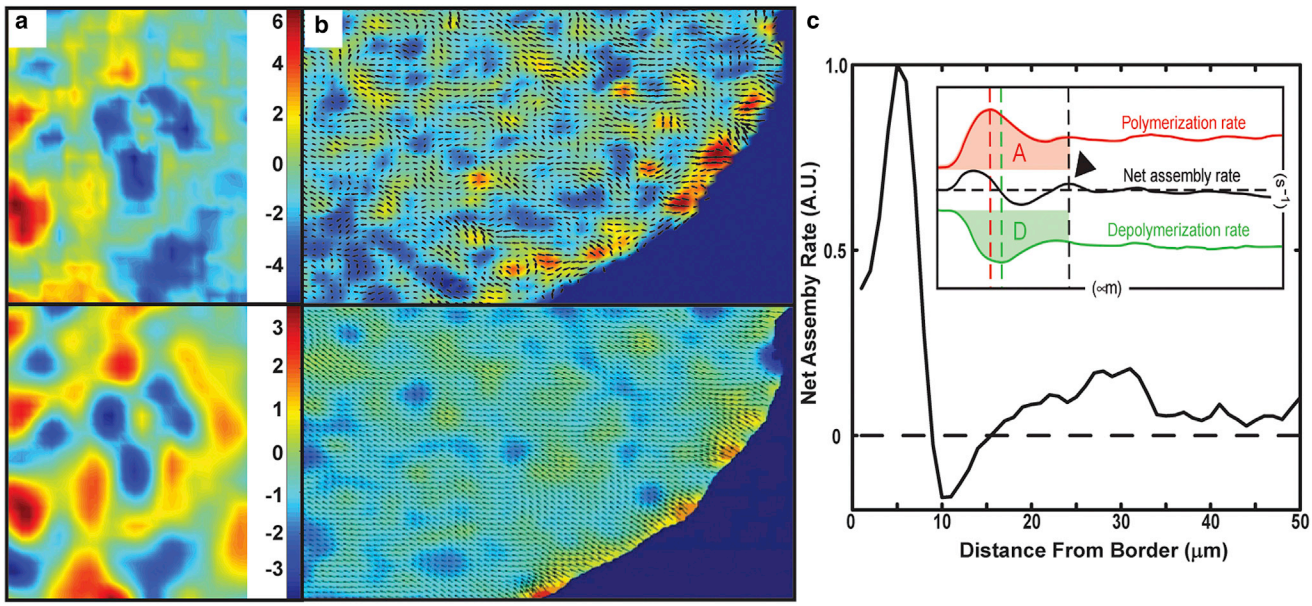

FIGURE 4 Measuring F-actin flow and polymerization rates using optical flow. (*a*) The accuracy of measuring net assembly rates by adding a reaction term in optical flow was determined by comparing the known net polymerization rate of fluorescent synthetic particles (*top panel*) with one calculated using the augmented version of optical flow (*bottom panel*). The root mean square of the error between the computed and known polymerization rates normalized by the root mean square of the known polymerization rate is 0.5. (*b*) The flow of F-actin in newt lung epithelial cells was computed using optical flow augmented with a reaction term (*top panel*) and speckle tracking (*bottom panel*, from Ponti et al. (9)). Arrows show velocity vectors and colors represent the flow speed. (*c*) The net assembly rate of F-actin as a function of distance from the border that was calculated using optical flow agrees well with Ponti et al.'s (9) data that illustrate the rate profiles (s^{-1}) as a function of distance (microns) (*inset*, *black line*). The bottom panel of (*b*) and inset in (*c*) are reprinted with permission from *Science* and Gaudenz Danuser. To see this figure in color, go online.

Although other groups are using optical flow constraint to investigate speckle flow (3,26), as well as extending the method for use with DIC microscopy (31), optical flow is still not commonly used within the biophysics and cell biology communities. To this end, we have provided a workflow of the optical flow constraint algorithm in Data S1 along with the MATLAB code (Data S2) and an instruction manual. But there is a much broader statement that should be made here. More and more, researchers are looking to live-cell imaging to provide a quantitative understanding of cellular mechanisms. Image processing is crucial to make sense of the vast data contained within these images. Therefore, it is necessary for us to make a greater effort to familiarize ourselves with work from the computer vision community (32). If we, as a community, do not make a conscious effort to bridge the gap between cell biology and computer vision, we may end up, in the best-case scenario, wasting time generating less accurate data, and, more critically, we may completely miss mechanistic features contained in our movies.

SUPPORTING MATERIAL

Supporting Materials and Methods, one figure, five movies, and two data files are available at http://www.biophysj.org/biophysj/supplemental/S0006-3495(16)30033-9.

ACKNOWLEDGMENTS

We thank Jean Wilson for providing MDCK I epithelial cells and G. Danuser for permission to use data shown in Fig. 4.

This research was supported by grants from the National Institutes of Health (R01 GM072004 to C.W.W. and training grant GM0884905 to D.K.V.) and the National Science Foundation (CMMI 1361987 to C.W.W.).

REFERENCES

1. Poujade, M., E. Grasland-Mongrain, …, P. Silberzan. 2007. Collective migration of an epithelial monolayer in response to a model wound. *Proc. Natl. Acad. Sci. USA*. 104:15988–15993.
2. Danuser, G., and C. M. Waterman-Storer. 2006. Quantitative fluorescent speckle microscopy of cytoskeleton dynamics. *Annu. Rev. Biophys. Biomol. Struct.* 35:361–387.
3. Vallotton, P., S. L. Gupton, …, G. Danuser. 2004. Simultaneous mapping of filamentous actin flow and turnover in migrating cells by quantitative fluorescent speckle microscopy. *Proc. Natl. Acad. Sci. USA*. 101:9660–9665.
4. Ng, M. R., A. Besser, …, J. S. Brugge. 2012. Substrate stiffness regulates cadherin-dependent collective migration through myosin-II contractility. *J. Cell Biol.* 199:545–563.
5. Bise, R., T. Kanade, Z. Yin, and S. I. Huh. 2011. Automatic cell tracking applied to analysis of cell migration in wound healing assay. *Conf. Proc. IEEE Eng. Med. Biol. Soc.* 2011:6174–6179.
6. Westerweel, J., G. E. Elsinga, and R. J. Adrian. 2013. Particle image velocimetry for complex and turbulent flows. *Annu. Rev. Fluid Mech.* 45:409–436.
7. Raffel, M., C. E. Willert, …, J. Kompenhans. 2014. Particle Image Velocimetry: A Practical Guide. Springer, Berlin/Heidelberg.
8. Ishihara, K., P. A. Nguyen, …, T. J. Mitchison. 2014. Microtubule nucleation remote from centrosomes may explain how asters span large cells. *Proc. Natl. Acad. Sci. USA*. 111:17715–17722.
9. Ponti, A., M. Machacek, …, G. Danuser. 2004. Two distinct actin networks drive the protrusion of migrating cells. *Science*. 305:1782–1786.
10. Petitjean, L., M. Reffay, …, P. Silberzan. 2010. Velocity fields in a collectively migrating epithelium. *Biophys. J.* 98:1790–1800.
11. Weiger, M. C., V. Vedham, …, C. A. Parent. 2013. Real-time motion analysis reveals cell directionality as an indicator of breast cancer progression. *PLoS One*. 8:e58859.
12. Supatto, W., D. Débarre, …, E. Beaurepaire. 2005. In vivo modulation of morphogenetic movements in Drosophila embryos with femtosecond laser pulses. *Proc. Natl. Acad. Sci. USA*. 102:1047–1052.
13. Dombrowski, C., L. Cisneros, …, J. O. Kessler. 2004. Self-concentration and large-scale coherence in bacterial dynamics. *Phys. Rev. Lett.* 93:098103.
14. Wioland, H., F. G. Woodhouse, …, R. E. Goldstein. 2013. Confinement stabilizes a bacterial suspension into a spiral vortex. *Phys. Rev. Lett.* 110:268102.
15. Brangwynne, C. P., C. R. Eckmann, …, A. A. Hyman. 2009. Germline P granules are liquid droplets that localize by controlled dissolution/condensation. *Science*. 324:1729–1732.
16. Style, R. W., R. Boltyanskiy, …, E. R. Dufresne. 2014. Traction force microscopy in physics and biology. *Soft Matter*. 10:4047–4055.
17. Lucas, B. D., and T. Kanade. 1981. An iterative image registration technique with an application to stereo vision. Proceedings of Imaging Understanding Workshop, pp. 121–130.
18. Jaqaman, K., D. Loerke, …, G. Danuser. 2008. Robust single-particle tracking in live-cell time-lapse sequences. *Nat. Methods*. 5:695–702.
19. Meinhart, C. D., S. T. Wereley, and J. G. Santiago. 2000. A PIV algorithm for estimating time-average velocity fields. *J. Fluids Eng.* 122:285–289.
20. Ji, L., and G. Danuser. 2005. Tracking quasi-stationary flow of weak fluorescent signals by adaptive multi-frame correlation. *J. Microsc.* 220:150–167.
21. Anandan, P. 1989. A computational framework and an algorithm for the measurement of visual motion. *Int. J. Comput. Vis.* 2:283–310.
22. Ruhnau, P., T. Kohlberger, …, H. Nobach. 2005. Variational optical flow estimation for particle image velocimetry. *Exp. Fluids*. 38:21–32.
23. Horn, B. K. P., and B. G. Schunck. 1981. Determining optical flow. *Artif. Intell.* 17:185–203.
24. Chetverikov, D., M. Nagy, and J. Verestoy. 2000. Comparison of tracking techniques applied to digital PIV. *Proc. Int. Conf. Pattern Recognit.* 4619:4619–4623.
25. Thielicke, W. S. E. 2014. PIVlab—towards user-friendly, affordable and accurate digital particle image velocimetry in MATLAB. *J. Open Res. Softw.* 2:2–10.
26. Wilson, C. A., M. A. Tsuchida, …, J. A. Theriot. 2010. Myosin II contributes to cell-scale actin network treadmilling through network disassembly. *Nature*. 465:373–377.
27. Reffay, M., M. C. Parrini, …, P. Silberzan. 2014. Interplay of RhoA and mechanical forces in collective cell migration driven by leader cells. *Nat. Cell Biol.* 16:217–223.
28. Maruthamuthu, V., B. Sabass, …, M. L. Gardel. 2011. Cell-ECM traction force modulates endogenous tension at cell-cell contacts. *Proc. Natl. Acad. Sci. USA*. 108:4708–4713.
29. Liu, T., and L. Shen. 2008. Fluid flow and optical flow. *J. Fluid Mech.* 614:253–291.
30. Brox, T., A. Bruhn, …, J. Weickert. 2004. High accuracy optical flow estimation based on theory for warping. *Proc. 8th Eur. Conf. Comput. Vis.* 4:25–36.
31. Danuser, G., P. T. Tran, and E. D. Salmon. 2000. Tracking differential interference contrast diffraction line images with nanometre sensitivity. *J. Microsc.* 198:34–53.
32. Danuser, G. 2011. Computer vision in cell biology. *Cell*. 147:973–978.